# Optimal mascon geometry in estimating mass anomalies within Greenland from GRACE

Ran, Jiangjun; Ditmar, Pavel; Klees, Roland

**DOI**
10.1093/gji/ggy242

**Publication date**
2018

**Document Version**
Final published version

**Published in**
Geophysical Journal International

Geophysical Journal International

*Geophys. J. Int.* (2018) **214,** 2133–2150
Advance Access publication 2018 June 20
GJI Gravity, geodesy and tides

doi: 10.1093/gji/ggy242

# Optimal mascon geometry in estimating mass anomalies within Greenland from GRACE

Jiangjun Ran, Pavel Ditmar and Roland Klees

*Delft University of Technology, Stevinweg* 1, 2628 *CN, Delft, the Netherlands. E-mail: j.ran@tudelft.nl*

Accepted 2018 June 19. Received 2018 June 7; in original form 2017 June 05

## ABSTRACT

The mascon approach is a well-known technique to estimate mass anomalies in Greenland using Gravity Recovery and Climate Experiment (GRACE) satellite gravity data. It partitions the area of interest into laterally homogeneous patches (mascons). An important aspect of the mascon approach is the chosen geometry of mascons. So far, its impact has not been fully understood. In this study, we use a full-scale numerical study and real data analysis to identify the optimal strategy (primarily, the size of the mascons) for the extraction of mass anomalies over the Greenland drainage systems from GRACE monthly solutions. We use ordinary and weighted least-squares techniques to estimate the mascon parameters. The weighted least-squares estimator uses the full noise covariance matrices of monthly GRACE models, that is, designed to suppress random noise in the estimates. In addition, the zero-order Tikhonov regularization is applied. Four types of quantities of interest, which are associated with different temporal scales, are investigated in this study: monthly mass anomalies, mean mass anomalies per calendar month, interannual mass variations and long-term linear trends. We show that the dominant error sources are random errors and parametrization (model) errors (PEs), as well as the bias introduced by the regularization. Errors in long-term linear trend estimates are dominated by PEs, whereas the role of random errors increases with the decreasing temporal scale. The best solutions are obtained when the territory of Greenland is split into at least 23 mascons (the area of each one being $\sim$90 000 km$^2$). The usage of smaller mascons does not worsen the solutions in most cases, which is explained by the application of the regularization. Usage of larger mascons leads in most cases to inferior results due to the impact of PEs. The application of the weighted least-squares estimator noticeably improves the quality of the solutions, with the exception of long-term linear trends estimated at the drainage system scale. In addition, we considered the long-term linear trend estimates integrated over entire Greenland. It is shown that the best results are obtained in that case when no regularization is applied. The results of real GRACE data processing are consistent with those obtained in the numerical study.

**Key words:** Gravity anomalies and Earth structure; Global change from geodesy; Satellite gravity.

## 1 INTRODUCTION

Mass variations in Greenland attract the attention of the scientific community because of the large potential to exacerbate future sea level rise. The Gravity Recovery and Climate Experiment (GRACE) satellite mission is one of the most valuable sources of information about those mass variations (Chen *et al.* 2006; Velicogna & Wahr 2006; Velicogna 2009; Jacob *et al.* 2012; Shepherd *et al.* 2012; Stocker *et al.* 2013; Schrama *et al.* 2014; Velicogna *et al.* 2014; Khan *et al.* 2015).

In this study, we analyse the estimation of mass variations in Greenland from GRACE data using the mascon (mass concentration) approach. Nowadays, this is a commonly used way to transform GRACE data into mass anomalies (Forsberg & Reeh 2007; Baur & Sneeuw 2011; Schrama & Wouters 2011; Schrama *et al.* 2014). In this approach, the target area is split into laterally homogeneous patches, which are called 'mascons'. The accuracy of the estimates obtained in this way is sensitive to the parameterization of the target area, that is, to the choice of the number and the geometry of the mascons (Bonin & Chambers 2013). Different parameterizations of the territory of Greenland have been used so far in literature. For instance, Luthcke *et al.* (2006) identified six

drainage systems and split each of them into two mascons, one for the area below the 2000 m elevation line and the other one for the area above the 2000 m elevation line. This rather coarse parameterization is not able to fully exploit the spatial resolution of GRACE. Therefore, finer parameterizations using mascons of a regular shape (e.g. equiangular mascons, equal-area mascons or spherical caps) have been proposed (Rowlands *et al.* 2005; Baur & Sneeuw 2011; Luthcke *et al.* 2013; Schrama *et al.* 2014; Watkins *et al.* 2015).

Up to now, it is common to choose the size of the mascons independently of the temporal scale under consideration. However, such an approach may be suboptimal. The primary goal of this study is to investigate the optimal choice of the mascon size depending on the type of the estimates. We consider four types associated with different temporal scales:

(1) Long-term linear trends (long-term temporal scale).
(2) Interannual mass anomalies (intermediate scale).
(3) Mean mass anomalies per calendar month (can also be considered as an intermediate scale, but based on an alternative way of averaging original information).
(4) Monthly mass anomalies (short-term scale).

The variant of the mascon approach presented in Ran *et al.* (2018a) is used in this study to compute the statistically optimal estimates of mass anomalies. Furthermore, we exploit the procedure proposed by Ran *et al.* (2018a) to subdivide Greenland into nearly equal-area mascons of a desired size, taking the coast geometry into account. In order to better understand the link between the accuracy of the obtained estimates and the selected parameterization, we start from a numerical study, where individual error sources are quantified. This allows us to make a proper interpretation of the results obtained from real GRACE data at the second stage and supports our recommendations regarding the optimal choice of parameterization.

It is important to note that only ∼81 per cent of the territory of Greenland is occupied by the Greenland Ice Sheet (GrIS). The rest is covered by tundra and isolated glaciers. In view of the limited spatial resolution of GRACE, the latter also contribute to GRACE-based estimates (unless the mass variations outside the GrIS are corrected for using hydrological models). Therefore, we refer to mass anomalies in Greenland rather than to GrIS mass anomalies throughout this study.

The rest of the paper is organized as follows. In Section 2, we briefly introduce the different parameterizations used in this study. In Section 3, we present a numerical study based on simulated signal and data. In Section 4, we analyse real GRACE data. Finally, in Section 5, we provide a summary and the conclusions.

## 2 METHODOLOGY AND PARAMETERIZATION

### 2.1 Adopted mascon approach

The adopted variant of the mascon approach (Ran *et al.* 2018a) stems from the methodology proposed by Forsberg & Reeh (2007) and Baur & Sneeuw (2011). First, we use the differences between monthly spherical harmonic coefficients (SHCs) and their long-term mean values to synthesize gravity disturbances at satellite altitude. The data area comprises the entire Greenland extended with a buffer zone of 800 km width. Numerical studies in Ran *et al.* (2018a) demonstrated that such a buffer zone is the best choice. Second, we compute a design matrix ($\mathbf{A}$) that links the gravity disturbances ($\mathbf{d}$) at satellite altitude to the mass anomalies of the mascons (mascon parameters, $\mathbf{x}$). Importantly, each column of the design matrix is computed by taking into account that data and mascon model must be spectrally consistent (Ran *et al.* 2018a). More specifically, each column of the design matrix could be treated as a set of gravity disturbances caused by the corresponding mascon of unit surface density. The computation is performed in three steps. First, the gravity disturbances are computed on an equiangular global grid. Second, a set of SHCs is computed by means of the spherical harmonic analysis. Third, the produced SHCs are used to compute spectrally limited gravity disturbances at the predefined data points.

Finally, we estimate the mascon parameters using the weighted least-squares technique (Eq. 1). The weight matrices ($\mathbf{C_d}^{-1}$) are taken as a pseudo-inverse of the noise covariance matrices of gravity disturbances. The latter are computed from the full noise covariance matrices of SHCs using the law of covariance propagation. The data weighting using these matrices may significantly reduce random noise (Ran *et al.* 2018a). In addition, similar to Schrama & Wouters (2011) and Bonin & Chambers (2013), we apply the zero-order Tikhonov regularization to stabilize the normal matrix and reduce noise in the estimates:

$$\mathbf{x} = (\mathbf{A}^T\mathbf{C_d}^{-1}\mathbf{A} + \alpha\mathbf{R})^{-1}\mathbf{A}^T\mathbf{C_d}^{-1}\mathbf{d}, \quad (1)$$

where the regularization matrix $\mathbf{R}$ is the unit one and $\alpha$ is the regularization factor, which is determined by the L-curve method (Hansen 1992).

However, random noise may not be the dominant error source (at least, at some of the temporal scales considered in this study). Therefore, we also use the ordinary least-squares techniques to estimate the mascon parameters.

### 2.2 Parameterization of Greenland

The parameterizations considered in this study are designed using the procedure of Ran *et al.* (2018a) and comprise almost equal-area mascons of a prescribed size. In this way, the whole Greenland is partitioned into 23 mascons (the area of each one being ∼90 000 km$^2$), 36 mascons (∼62 500 km$^2$) or 54 mascons (∼40 000 km$^2$) (cf. Figs 1d–f). In addition, we consider three other parameterizations, which are frequently used in the literature: with 6 mascons (Luthcke *et al.* 2006), 8 mascons (Zwally *et al.* 2012) and 12 mascons (Luthcke *et al.* 2006) (Figs 1a–c). Note that the divisions into six and eight mascons follow the geometry of major drainage systems. The Greenland mascons are complemented by nine mascons outside Greenland to reduce the inward signal leakage from regions around Greenland (Yi *et al.* 2016; Ran *et al.* 2018a).

## 3 NUMERICAL STUDY

To understand the impact of the parameterization on the accuracy of estimated mass variations at different temporal scales, and to understand how errors from different sources compare with each other, a series of numerical experiments are conducted with synthetic data. The experimental set-up and the results are presented in Sections 3.1 and 3.2, respectively.

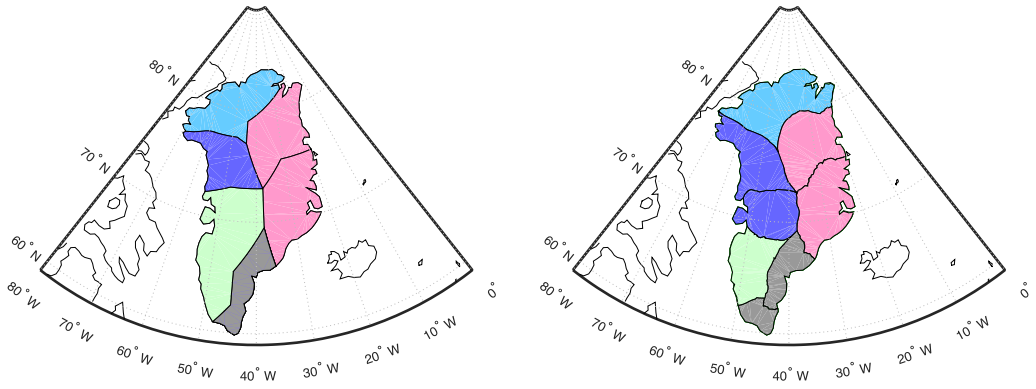


(a) 6 mascons




(b) 8 mascons

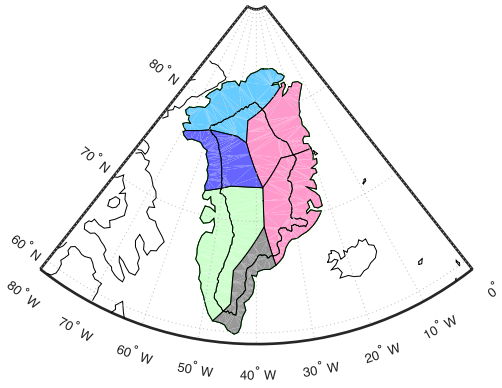


(c) 12 mascons

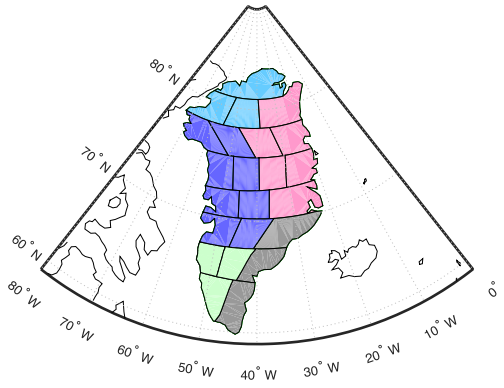


(d) 23 mascons

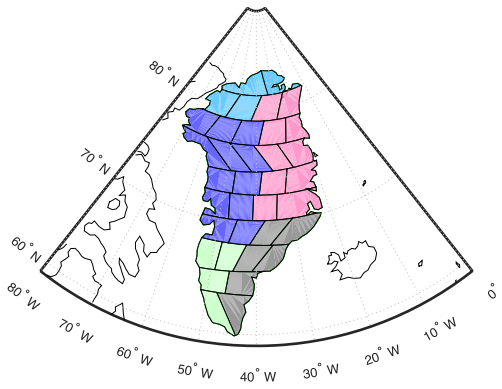


(e) 36 mascons

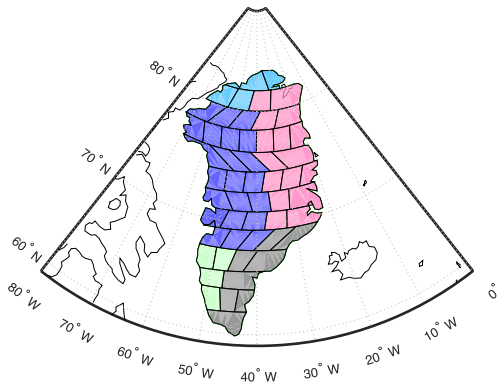


(f) 54 mascons

**Figure 1.** The parameterizations of Greenland considered in this study. Greenland is divided into five regions, which are aggregated from mascons. The regions approximately follows the geometry of five drainage systems, which are outlined with different colours, that is, north (N) in light blue, northeast (NE) in red, southeast (SE) in grey, southwest (SW) in green, and northwest (NW) in blue.

### 3.1 Experimental set-up

The basic set-up includes the definition of the true signal and the definition of the individual error sources considered in the simulations.

#### *3.1.1 'True' signal*

The 'true' signal is composed of a long-term linear trend and other temporal variations. The long-term trend is based on ICESat laser altimetry estimates over the period 2003–2009. Their spatial resolution is 20 × 20 km (Felikson *et al.* 2017). By assuming the density of the material responsible for elevation changes to be 917 kg m$^{-3}$ (Wahr *et al.* 2000), the elevation change rates are converted into

mass change rates in terms of equivalent water heights (EWH) (Fig. 2). The linear trend over the tundra area is set equal to zero. The integration of the obtained trends over entire Greenland results in the value of $-110$ Gt yr$^{-1}$, which is much lower than that based on GRACE data over the period 2003–2013, about $-286$ Gt yr$^{-1}$ (Ran *et al.* 2018a). To make the ICESat-based estimates more realistic, we upscale all of them with a single scale factor of 2.6. A similar upscaling procedure was applied earlier by Bonin & Chambers (2013).

The other simulated mass variations are based on surface mass balance (SMB) time-series from the RACMO 2.3 model (Noël *et al.* 2015). The spatial resolution is about 11 $\times$ 11 km, whereas the temporal sampling is 1 d. The output from RACMO 2.3 during the time interval 2003–2013 was integrated over time to produce daily mass anomalies. After this, we computed monthly mass anomalies, re-sampled them to the 20 $\times$ 20 km patches in order to make them consistent with the ICESat data, and de-trended. The resulting time-series describe predominantly seasonal mass variations (their annual amplitudes are shown in Fig. 2). Then, we combined the de-trended signal with the trend from ICESat to form the 'true' signal. Note that the 'true' signal over the tundra area lacks long-term trends and, therefore, is dominated by seasonal variations.

The 'true' mass anomalies defined at the 20 $\times$ 20 km blocks were used to compute gravity disturbances on an equiangular global grid at satellite altitude. The gravity disturbances were expanded in spherical harmonics complete to some maximum degree (namely, degree 96) using spherical harmonic analysis. Finally, the truncated spherical harmonic model was used to generate spectrally limited gravity disturbances, which represent the error-free data. The spectral content of the simulated data is similar to that of real GRACE data. Furthermore, the procedure applied to compute the simulated data is basically the same as the one to compute the design matrix (Section 2.1). This assures the spectral consistency between the data and the mascon model. In the absence of the spectral consistency, the estimated mass anomalies may suffer from large errors, particularly when the optimal data weighting is applied Ran *et al.* (2018a).

#### 3.1.2 Simulated noise

Different types of errors are added to the 'true' signal: signal leakage, AOD noise and random noise. In addition, PEs, sometimes referred to as 'model errors' (Stedinger & Tasker 1986; Xu 2010), are automatically included due to the much higher spatial resolution of the 'true' signal compared to the size of the mascons.

*Signal leakage.* Signal leakage refers in this study to the signal from mass anomalies outside Greenland (e.g. the Canada's Arctic Archipelago glaciers, the North Canada, Iceland, Svalbard, etc. see Fig. 3), which may disturb the estimates of mass anomalies in Greenland (i.e. inward signal leakage is meant). To include leakage errors, we generated mass variations in surrounding land areas using GRACE monthly land water mass grids from GRACE Tellus (Swenson 2012). In line with the time interval of the 'true' signal, we considered 123 monthly solutions over the period 2003–2013 (9 months were excluded from the data processing due to lack of data). The simulated trends and annual amplitudes extracted from monthly GRACE Tellus solutions over the mascons located outside Greenland are shown in Fig. 3.

*AOD noise.* Uncertainties in the background models that are used to produce monthly GRACE solutions may cause inaccuracies in the mass variation estimates. One of such background models is the Atmosphere and Ocean De-aliasing model release 05 (AOD) (Dobslaw *et al.* 2013). Here, we defined AOD errors as 10 per cent of the mean monthly signal (Thompson *et al.* 2004; Ditmar *et al.* 2012).

*Random noise.* Random noise in monthly GRACE solutions was generated from the noise covariance matrices of monthly GRACE solutions provided by CSR. It contains north–south stripes, which vary by latitude and from month to month as noise stripes in real GRACE data do. We produced multiple different realizations of random noise, one realization per month. Ideally, this needs to be done per month using the corresponding noise covariance matrix. However, such an approach is very time consuming, especially when using a weighted least-squares estimator. Therefore, we chose the noise covariance matrix of June 2008 as a representative, and generated for each month noise realizations based on this noise covariance matrix.

*Parameterization error.* The actual mass anomaly distribution is a continuous function, whereas the mascon approach assumes a uniform mass distribution within each mascon. This inconsistency may introduce parameterization errors (also called 'model errors'). In other words, the parameterization error represents the disturbances caused by replacing the actual mass anomaly distribution with a single mean value per mascon. The parameterization error (PE) of a mascon in terms of surface density could be mathematically defined as:

$$\mathrm{PE}(\phi, \lambda) = \rho(\phi, \lambda) - \bar{\rho}, \tag{2}$$

where $\rho(\phi, \lambda)$ is the density of mass anomaly at gridpoint $(\phi, \lambda)$ inside the mascon, while $\bar{\rho}$ is the mean density. Eq. (2) provides the input to compute the parameterization error in terms of gravity disturbances, consistently with other errors. In our study, incorporation of parameterization errors takes place in a natural way, since the 'true' signal is defined over 20 $\times$ 20 km patches, which are much smaller than the size of the mascons. In the simulations without parameterization errors, we define the 'true' signal per mascon as the sum of mass anomalies at all 20 $\times$ 20 km patches within the given mascon, which is homogeneously distributed over the mascon. Note that the parameterization errors in different months are different, since the simulated signal varies from month to month.

### 3.2 Results

In our study, we address (i) long-term linear mass variation rates, (ii) interannual mass anomalies, (iii) mean mass anomalies per calendar month and (iv) monthly mass anomalies. We investigate the impact of the parameterization on these estimates and select the best parameterization in each case. We conduct the analysis at the level of drainage systems. To that end, we divide Greenland into five regions, which approximately follow the geometry of the drainage systems defined in van den Broeke *et al.* (2009). The geometries of the regions that are aggregated from mascons are shown in Fig. 1. Note that it is not possible to make the geometries of the five drainage systems (as shown in Fig. 1 with different colours) to be exactly the same for different parameterizations. The impact of the differences between the resulting geometries is, however, minor, since we compare estimates over each drainage system with the 'true' value based

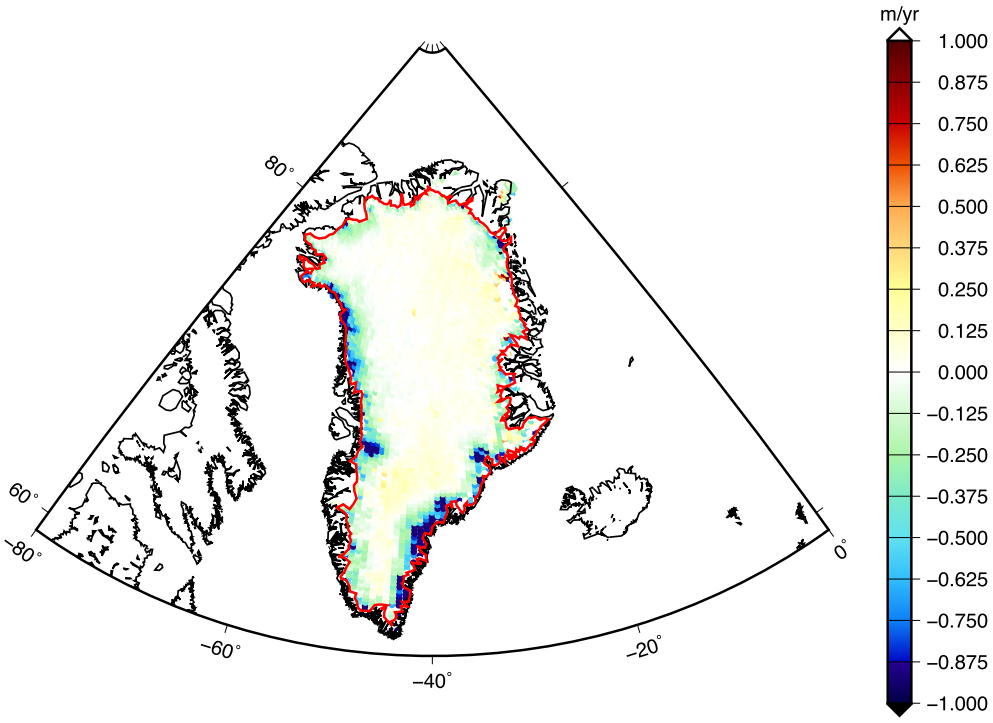


(a)

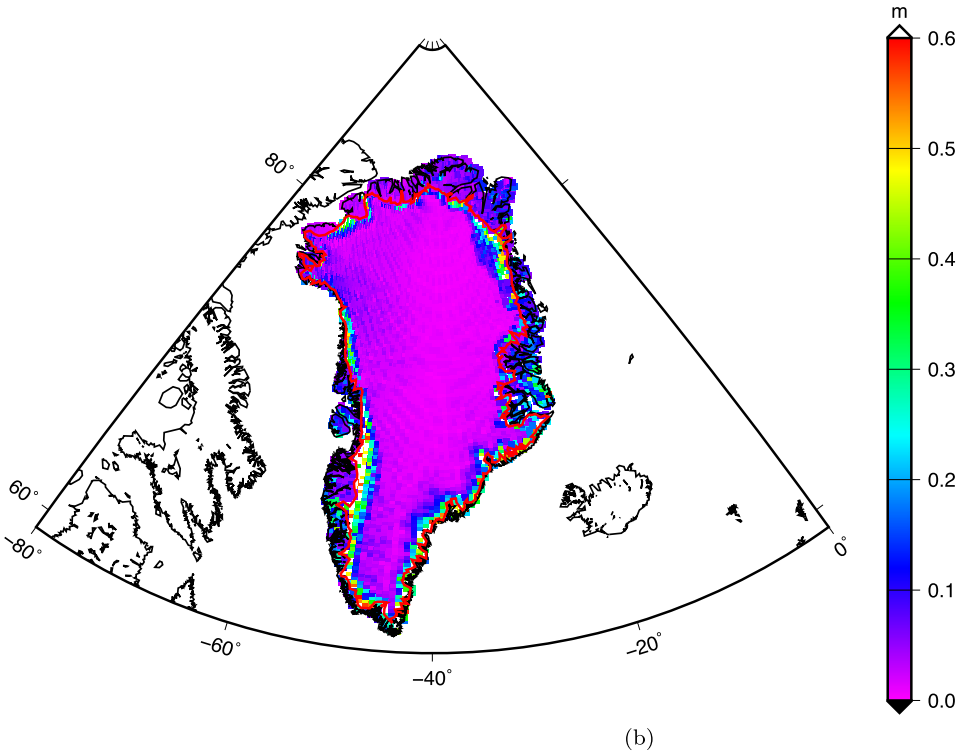


(b)

**Figure 2.** (a) GrIS mass change rate per 20 × 20 km patch from ICESat data over the period 2003–2009 (EWH: m yr$^{-1}$). The thick red curve is the ice mask, which indicates the boundary of the ice sheet. (b) Amplitude of annual mass variations over the entire Greenland for the period 2003–2013 extracted from RACMO2.3 (EWH: m).

on the same geometry. The estimates and rms errors in this study are provided in units of gigatransfers. Switching to equivalent water height in units of metres has no impact on the main conclusions of this study.

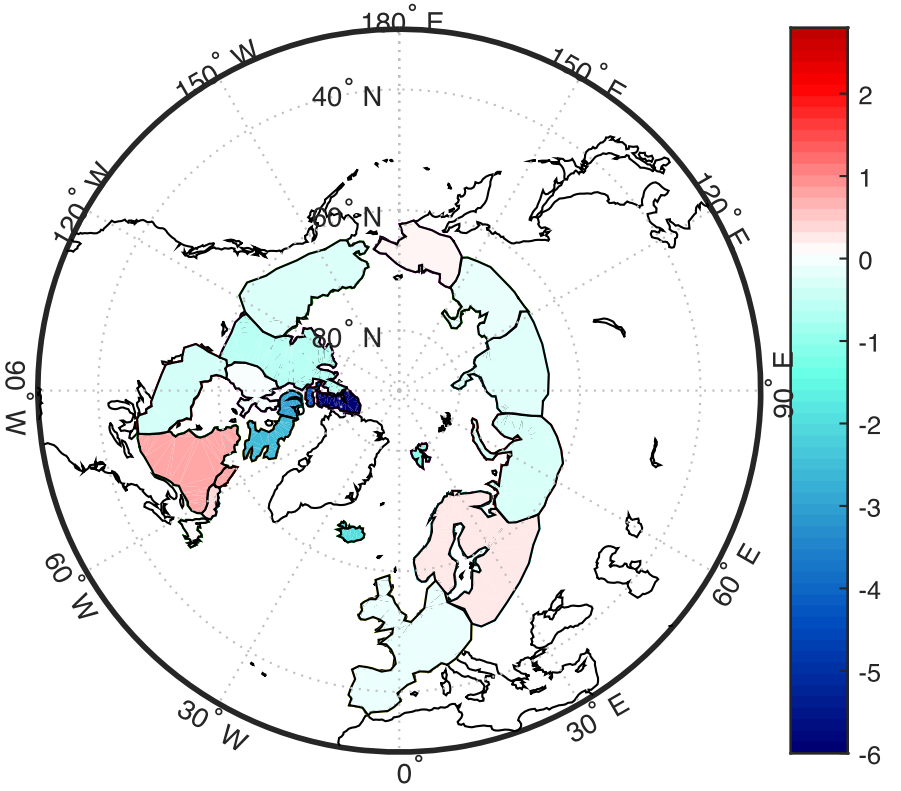


(a)

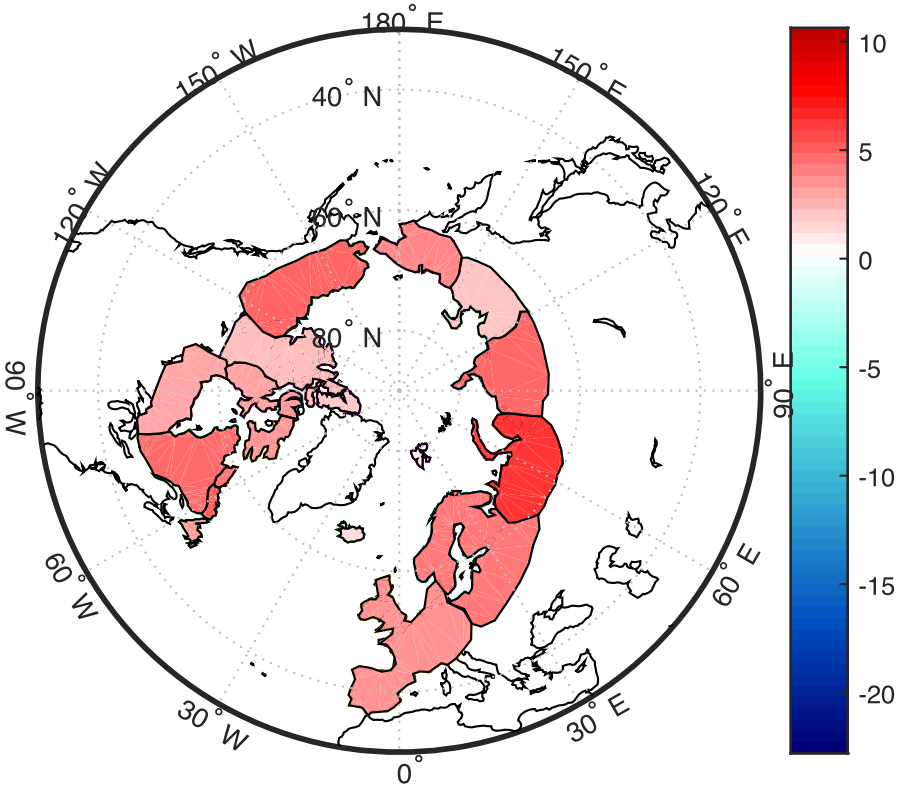


(b)

**Figure 3.** (a) Rate of linear mass changes for mascons outside Greenland (EWH: cm yr$^{-1}$). (b) The annual amplitude of mass change for those mascons outside (EWH: cm). The mascons outside Greenland are introduced to simulate the inward signal leakage.

As it is explained in Section 2.1, all the computations are performed using two estimators: (i) a weighted least-squares estimator and (ii) the ordinary least-squares estimator. The corresponding solutions are referred to as solutions with and without data weighting, respectively. When applying the weighted least-squares estimator, we compute the weight matrix based on the data noise covariance matrix of June 2008.

In our analysis, we address not only propagated noise, but also the bias introduced by the zero-order Tikhonov regularization. To quantify this bias, we invert error-free data and take the difference between the obtained estimates and the true signal. When analysing the contribution of an individual error source to the total error budget, one should subtract the bias to avoid its 'double-booking'. The bias in the estimates usually increases rapidly with the regularization factor. Please see Section 3.2.1 for further discussion.

The optimal regularization parameter is defined separately for each parameterization and each type of estimates (i.e. each timescale). To that end, we invert the simulated data with all the error sources switched on, trying different regularization parameters. The parameter that results in the smallest difference between the recovered estimates and the true signal is defined as the optimal one. Then, it is applied also in the scenarios when individual error sources are considered. This ensures a consistency of the obtained results and allows for their usage in the analysis of the total error budget.

### 3.2.1 *Recovery of long-term linear trends*

After summing up the recovered mass anomalies over all mascons within each drainage system, we extracted the linear trend ($t^{\text{recovered}}$) of mass change in Gt yr$^{-1}$, co-estimated with bias, annual and semi-annual terms. The true linear trend ($t^{\text{true}}$) at the drainage system scale was estimated from the true mass anomaly time-series. As quality measure, we use the rms difference between the estimated and true linear trends. This rms difference is referred to as the 'total rms error' if all error sources are included, and computed as:

$$\text{rms}_t = \sqrt{\frac{\sum_{n=1}^{5}(t_n^{\text{recovered}} - t_n^{\text{true}})^2}{5}}, \tag{3}$$

where $n$ represents the $n$th drainage system. If only a single noise source is considered, the corresponding rms difference is referred to as rms AOD error, rms leakage error, rms parameterization error and rms random error, respectively.

The total rms error as a function of total number of mascons is shown in Fig. 4. The smallest total rms error (∼6 Gt yr$^{-1}$) is obtained when the number of mascons ranges from 23 to 54, showing little difference within this range, no matter whether data weighting is switched on or not. As far as individual error sources are concerned, Fig. 4 reveals that the rms parameterization error is dominant when data weighting is used. If the data weighting is absent and number of mascons ≥23, the bias is comparable to or even exceeds the parameterization error. This is caused by the fact that the normal matrix for a large number of mascons is ill-posed (particularly, in the absence of data weighting, which reduces the condition number of normal matrix; see Fig. 5). Thereby, a strong regularization is needed to suppress propagated noise.

The rms random error in the estimated trends is rather small: ∼0.5 Gt yr$^{-1}$ and ∼1 Gt yr$^{-1}$ with and without data weighting, respectively. This is about an order of magnitude smaller than the rms parameterization error. The rms leakage error and the rms AOD error are either comparable to the rms random error or even smaller.

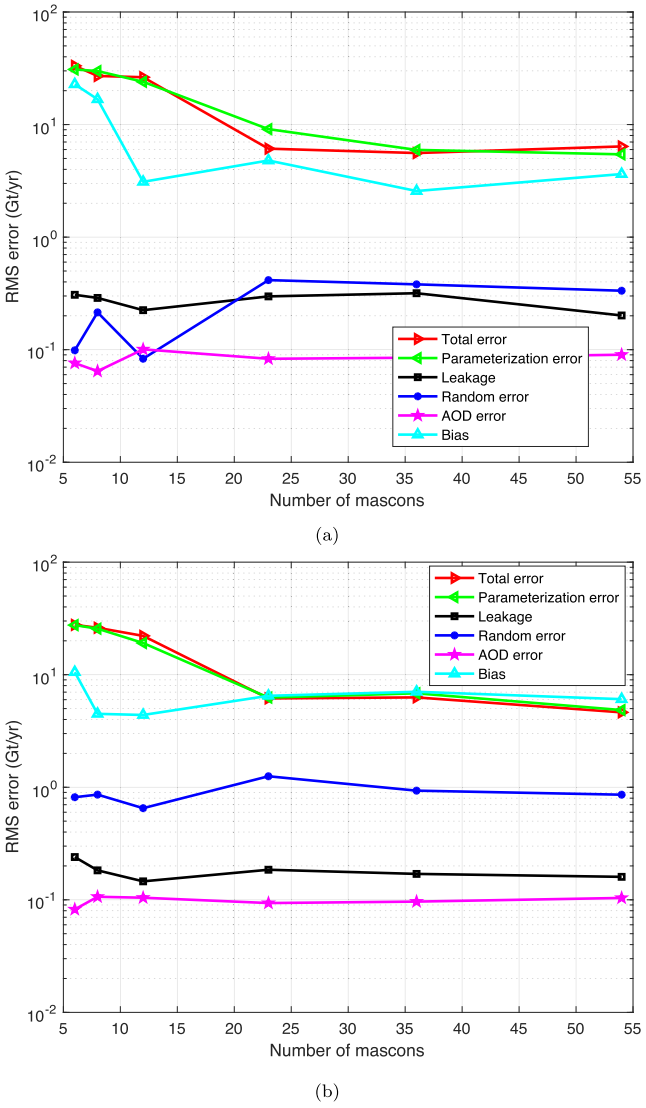


**Figure 4.** Total rms error and rms error of individual error sources of linear trends at drainage system scale in units of Gt yr$^{-1}$. Weighted least-squares estimator (a) versus ordinary least-squares estimator (b), as a function of the number of mascons.

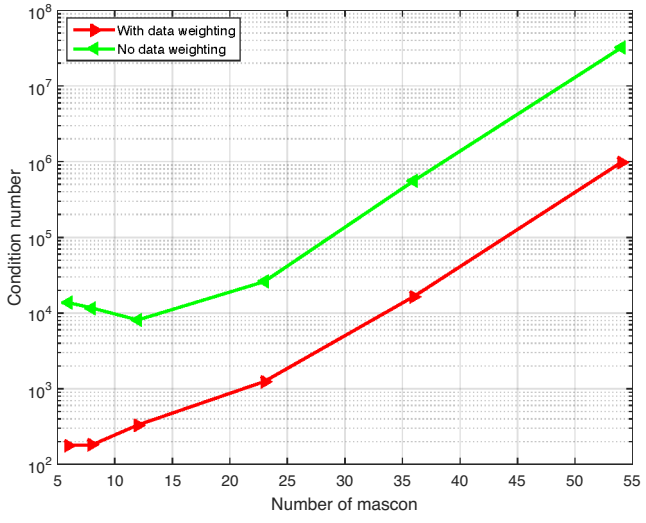


**Figure 5.** Condition numbers of the normal matrices when using the ordinary least-squares estimator (green) and weighted least-squares estimator (red), as functions of the number of mascons. Note that no regularization is used when computing the condition numbers.

Based on the results shown in Fig. 4, we conclude that if one is interested in the long-term linear trend at drainage system scale, data weighting is not necessary. The ordinary least-squares estimator provides comparable results. This is not surprising, since the data weighting is designed to suppress random noise, whereas the dominant contributor to the error budget is parameterization errors. The optimal number of mascon for trend estimates is in the range of 23–54.

In Fig. 6, we partitioned the error budget of trend estimates per mascon into individual error sources, when parameterizing Greenland with 23 mascons and switching on data weighting. In addition, the recovered and true trends per mascon are shown. The figure shows that in general the mascon approach is capable to recover the spatial pattern of mass anomalies in Greenland.

Next, we analyse the linear trend estimates integrated over entire Greenland. As an example, we take the parameterization with 23 mascons, which is one of the best parameterizations to estimate the trends at the drainage system scale, as discussed earlier. The impact of the regularization parameter on the trend estimates obtained both with and without data weighting is presented in Fig. 7. We note that, in the case of data weighting, the regularization biases the trend estimates by around 1 Gt yr$^{-1}$ if the regularization parameters are small and by ∼6 Gt yr$^{-1}$, if the regularization parameters are chosen to yield the best trend estimates at the drainage system scale. In addition, it is found that the bias rapidly increases with the regularization parameter, no matter whether data weighting is applied or not. Therefore, considering the larger total error of the regularized case (∼6 Gt yr$^{-1}$) compared to the unregularized case (∼1 Gt yr$^{-1}$), we suggest that a regularization is not applied when the trend for entire Greenland is estimated.

The results obtained with different parameterizations without a regularization are shown in Fig. 8. To begin with, we notice that the total rms error decreases with increasing number of mascons. The minimum is attained for a large number of mascons (i.e. larger than 23) no matter whether data weighting is used (−0.8 Gt yr$^{-1}$) or not (2.0 Gt yr$^{-1}$). If a small number of mascons is used, the total rms error may be very large, in particular when no data weighting is applied. For instance, when using just 6 mascons, the total rms error is ∼6 Gt yr$^{-1}$ with data weighting and ∼40 Gt yr$^{-1}$ without data weighting, respectively. The parameterization error is the dominant contributor to these large errors, whereas all the other errors are negligible.

We conclude that when estimating a linear trend for entire Greenland, one needs to take care that enough mascons (e.g. not less than 23) are used to reduce the parameterization error. The choice of a sufficiently large number of mascons is particularly important when the ordinary least-squares estimator is used. The highest quality is obtained when the weighted least-squares estimator is used in combination with a sufficiently large number of mascons.

### 3.2.2 *Recovery of inter-annual mass anomalies*

The inter-annual mass variations are another quantity of interest in the studies of the Greenland mass balance. In this section, we investigate the sensitivity of the estimated inter-annual mass variations to the chosen parameterization at the drainage system scale.

We start by removing the long-term trend from the time-series obtained for each mascon. After that, we compute the inter-annual mass variations, together with the mean mass anomalies per calendar month, which will be investigated in Section 3.2.3. To that end, we use the functional model

$$m^{i,j} = \overline{\widehat{m}}^{i} + \widehat{b}^{j}, \tag{4}$$

where $\{m^{i,j}: i = 1 \ldots 12, j = 1 \ldots J\}$ is the mass anomaly of month $i$ and year $j$, with $J$ being the number of years. $\widehat{b}^{j}$ is the mean anomaly of year $j$, which accounts for the inter-annual variability. And $\overline{\widehat{m}}^{i}$ is the mean mass anomalies of calendar month $i$. We added the constraint:

$$\sum_{i=1}^{12} \overline{\widehat{m}}^{i} = 0, \tag{5}$$

to guarantee the uniqueness of the solution. The $12 + J$ parameters per mascon are estimated using ordinary least-squares. The corresponding interannual variations for each drainage system are computed by a summation over all the mascons inside the drainage system.

The rms error of inter-annual mass variations per drainage system, IA, was computed as the rms difference between the estimated and the 'true' interannual mass variations of all years, that is,

$$\mathrm{IA} = \sqrt{\frac{\sum_{j=1}^{J} (b_j^{\mathrm{recovered}} - b_j^{\mathrm{true}})^2}{J}}. \tag{6}$$

Then, the rms error of inter-annual mass variations was computed as:

$$\mathrm{rms} = \sqrt{\frac{\sum_{k=1}^{5} \mathrm{IA}_k^2}{5}}. \tag{7}$$

This rms error was used to quantify the total rms error and rms error per error source for the estimates obtained both with and without data weighting. The results obtained for different parameterizations are shown in Fig. 9. The smallest total rms error (∼4 Gt) is obtained for 23 mascons with data weighting, which is slightly less than the smallest error (∼5 Gt) in the absence of data weighting. Note that a comparable quality is also found for a larger number of mascons (36–54 mascons). Regarding the individual error sources, the parameterization error is dominant only when the number of mascons is small (6–12 in the case with data weighting and 6 in the absence of data weigthing). In contrast, the random error, in general, increases with the number of mascons, and becomes the dominant error sources when the number of mascons is ≥36 (when the data weighting is applied) or ≥12 (without the data weighting). Note that the random error does not increase significantly with the number of mascons, which is caused by the spatial regularization. When the spatial regularization is switched off, the random error in the estimates increases significantly (not shown here). The bias stays at the levels comparable either with the random error or the parameterization error (depending on which one is larger). The leakage and AOD error are negligible: at the level of 0.4 Gt and 1 Gt, respectively.

Fig. 10 presents the 'true' and estimated interannual mass variations for each drainage system and for whole Greenland in the 23 mascon case, when data weighting is applied. The plot suggests that the recovered interannual mass variations are in a good agreement with the true ones. For completeness, the rms errors of the estimates obtained with and without data weighting, the rms of true inter-annual mass anomalies, and signal-to-noise ratios (SNRs) are shown in Table 1. The largest SNR (6.0) is obtained in the case of 23 mascons in combination with data weighting. Note that a comparable SNR is also observed for 36–54 mascons.

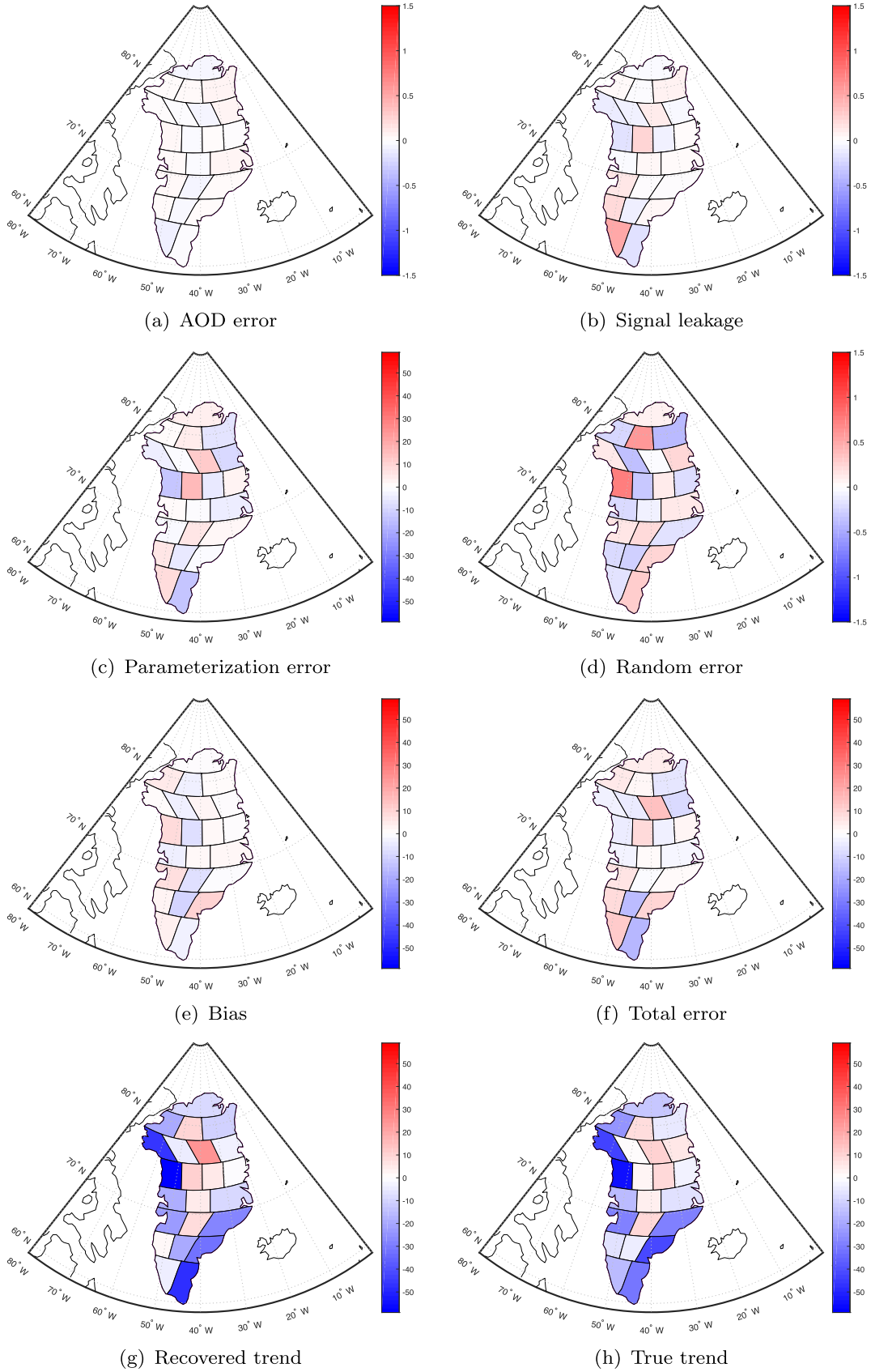


**Figure 6.** Contributors to the error in linear trend estimates: AOD error (a), signal leakage (b), parameterization error (c), random error (d), bias (e) and total error (f). For completeness, we also show the recovered trend (g) and true signal (h). The units are Gt $yr^{-1}$. Please note that, corresponding to the amplitude of the noise or signal levels, two different colour bars are used.

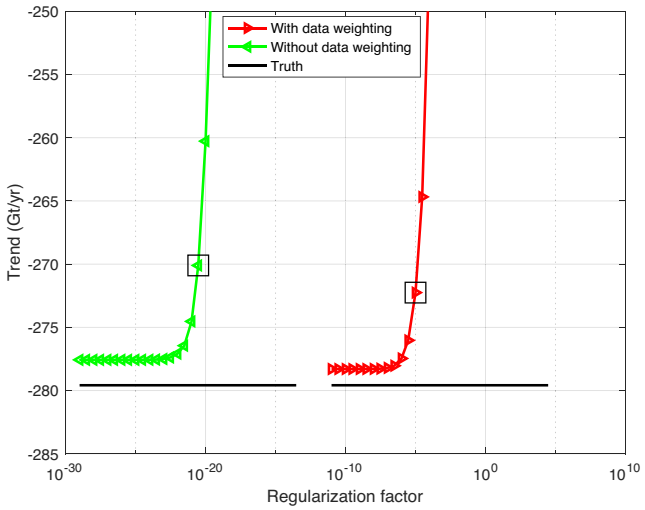


**Figure 7.** The impact of the regularization parameter on trend estimates integrated over entire Greenland, with and without data weighting. The true trend is shown in black, whereas the estimates obtained with the 'optimal' regularization parameters are highlighted as black squares. The 'optimal' regularization parameters are defined from the analysis of trend estimates at the drainage system scale.

From the analysis earlier, we conclude that parameterizing Greenland with 23–54 mascons in combination with data weighting provides the best inter-annual mass variation estimates.

### 3.2.3 *Recovery of mass anomalies per calendar month*

Mean mass anomalies per calendar month are useful to study the seasonal cycle of mass variations and the processes associated with it (Ran 2017). Here, we examine the impact of the parameterization on the accuracy of estimated mean mass anomalies per calendar month at the drainage system scale. Note that in line with Ran (2017), we do not remove the long-term variabilities from the estimated and the true time-series.

As it is already mentioned in Section 3.2.2, the mean mass anomalies per calendar month are extracted from the mass anomaly time-series as the least-squares solution of the system of linear equations given by Eqs (4) and (5). Note that the least-squares analysis is superior to the plain averaging of mass anomalies per calendar month over many years. This is because of the long-term variability, which has to be properly accounted for, in particular in the presence of data gaps. For instance, the absence of January data in a few years in succession may create a significant offset in the mean January value with respect to other months. The usage of a least-squares scheme solves this problem.

The rms error per drainage system, $\tau_k$, was computed as the rms difference between the estimated and the 'true' mean mass anomalies for all 12 months, that is,

$$\tau_k = \sqrt{\frac{\sum_{n=1}^{12}(\overline{m}_{k,n}^{\text{recovered}} - \overline{m}_{k,n}^{\text{true}})^2}{12}}, \tag{8}$$

where $\overline{m}_{k,n}^{\text{recovered}}$ and $\overline{m}_{k,n}^{\text{true}}$ are the estimated and true mean mass anomalies of the $k$th drainage system at month $n$, respectively. As an example, Fig. 11 shows the mean true mass anomalies per calendar month of the Northern (N) drainage system when using a parametrization comprising eight mascons.

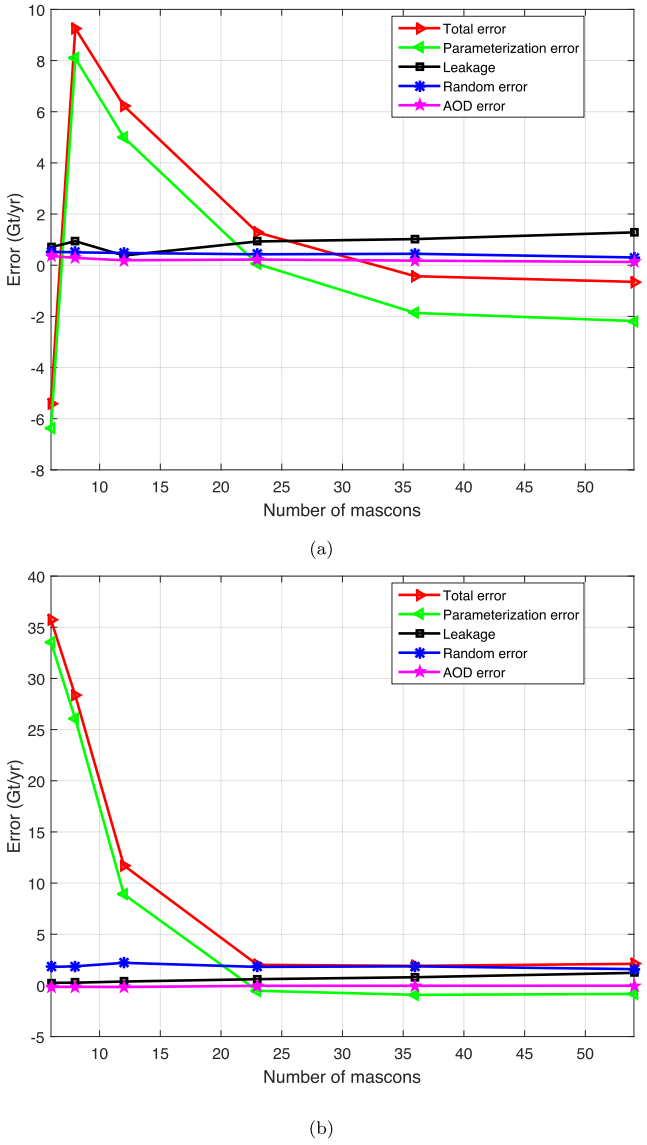


**Figure 8.** Errors in the linear trend (in Gt $\text{yr}^{-1}$) over entire Greenland obtained with the weighted least-squares estimator (a) and the ordinary least-squares estimator (b), respectively, as functions of the number of mascons.

Then, the rms error of mean mass anomalies per calendar month was computed as:

$$\text{rms}_{\overline{m}} = \sqrt{\frac{\sum_{k=1}^{5}\tau_k^2}{5}}. \tag{9}$$

The rms error of mean mass anomalies per calendar month computed as total rms error and as rms error per error source is shown for different parameterizations in Fig. 12. Obviously, using the data weighting provides a smaller total rms error, as compared to the ordinary least-squares adjustment (i.e., ∼6 Gt versus ∼8 Gt for 23 mascons). In addition, statistical information (the rms errors and signal, as well as SNRs) is shown in Table 2. The largest SNRs (∼6) is observed in the presence of data weighting, when the number of mascons is in the range from 23 to 54.

As far as the rms error per error source is concerned, we notice that no matter whether data weighting is used or not, the parameterization error decreases with increasing number of mascons, whereas the other errors show a minor sensitivity to the number of mascons.

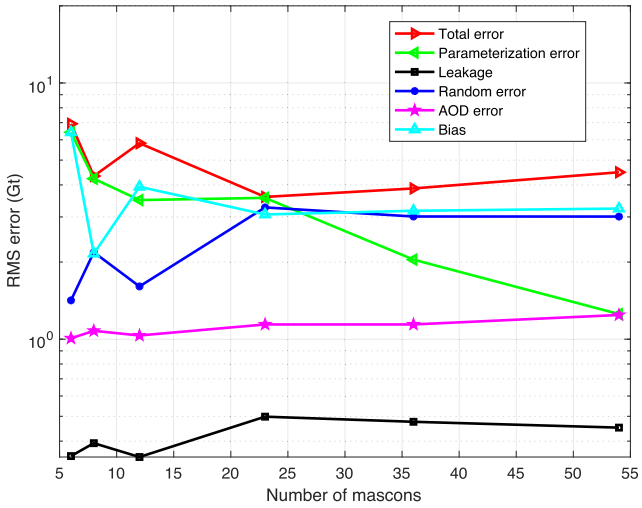


(a)

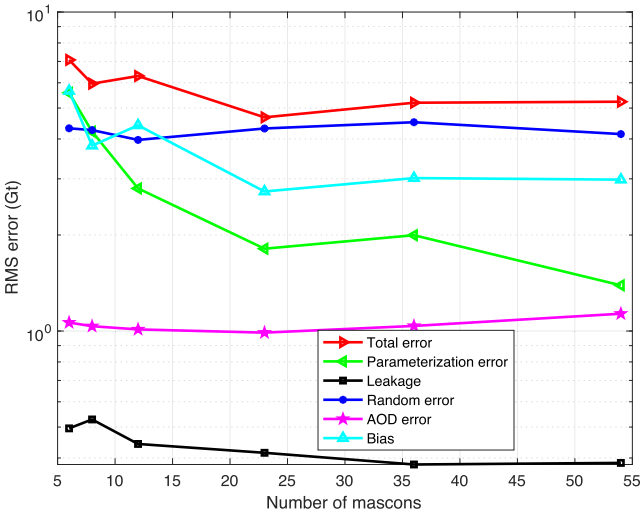


(b)

**Figure 9.** Total rms error and rms error of individual error sources of inter-annual mass variations at drainage system scale as functions of the number of mascons, in units of gigatransfers. Weighted least-squares estimator (a) versus ordinary least-squares estimator (b).

For a low number of mascons, the parameterization error is the dominant error source, whereas for finer parameterizations, the random error becomes dominant. The crossing points of the two error types are between 23 and 36 mascons and between 8 and 12 mascons for the weighted and ordinary least-squares estimators, respectively.

From the discussion earlier, we conclude that the best mean mass anomalies per calendar month are obtained when parameterizing Greenland with 23–54 mascon and switching data weighting on.

### *3.2.4 Recovery of monthly mass anomalies*

In this section, we analyse the impact of the parameterization on the accuracy of monthly mass anomaly estimates at the drainage system scale. We define the monthly mass anomalies as 'the residual signal left after removing the trend and interannual variability'. We de-trend and remove the inter-annual variability from both the estimated and the true time-series of monthly mass anomalies. The total rms error and the rms errors per error source are computed as the rms difference between the two residual time-series, that is,

$$\text{rms} = \sqrt{\frac{\sum_{n=1}^{N}(m_n^{\text{recovered}} - m_n^{\text{true}})^2}{N}}, \tag{10}$$

where $m_n$ is the mass anomaly of month $n$ and $N$ is the number of months.

Fig. 13 shows the results. In the presence of data weighting, the total rms error attains a minimum of ∼9 Gt when 23–54 mascons are used. Increasing the number of mascons does not increase the total rms error, which is explained by the usage of the spatial regularization. Without data weighting, the total rms error stays at a stable level of ∼17 Gt and is not sensitive to the number of mascons at all. In general, the total rms error is smaller by ∼50 per cent when data weighting is applied.

Table 3 shows that the SNR varies in a small range for the estimates obtained both with and without data weighting, reaching the maximum of 2.8 for the 23–54 mascons in the presence of data weighting. Fig. 14 shows the time-series estimated with data weighting in the 23 mascon case. Note that the $1-\sigma$ error bar is also shown. The results indicate that the monthly mass anomalies agree well with the true signal at the drainage system scale and even better when entire Greenland is considered.

When looking at the individual error sources, we see that the random error dominates the error budget in most cases. An exception is the estimates obtained in the 6-mascon case with data weighting, when the parameterization error plays the largest role. However, that error rapidly decreases as the number of mascons increases. The AOD error and leakage error are negligible.

## 4 ANALYSIS BASED ON REAL GRACE DATA

In this section, we investigate the impact of the parameterization on Greenland mass anomaly estimates based on real GRACE data. We use the RL05 GRACE monthly gravity field solutions from the Center for Space Research (CSR) at the University of Texas as input. Each solution is provided as a set of SHCs complete to degree 96, and supplied with a full noise covariance matrix. The considered time interval is January 2003–December 2013. Since data for 9 months were missing, the set comprises 123 months. Due to strong noise in the $C_{20}$ coefficients, we replace them with available estimates based on satellite laser ranging (Cheng *et al.* 2013). The degree-one coefficients, which are missing in the GRACE products, are taken from Swenson *et al.* (2008). In addition, the GRACE solutions are corrected for glacial isostatic adjustment (GIA) using the model from A *et al.* (2013). For each parameterization, a time-series of mass anomalies per mascon is obtained with the optimal regularization factor, which is determined using the L-curve method (Hansen 1992). These time-series are used as input for the further analysis.

### 4.1 Analysis of long-term linear trends

First, we investigate the impact of the parameterization on the long-term linear trend estimates at the drainage system scale. From the numerical study, we know that the trend estimates obtained using 23 mascons reach the highest level of quality. Therefore, this parameterization is used in our further analysis. To begin with, we sum up the mass anomalies per mascon over each drainage system, and extract the linear trend, co-estimated with a bias, annual and semi-annual terms. The obtained trend estimates are presented in

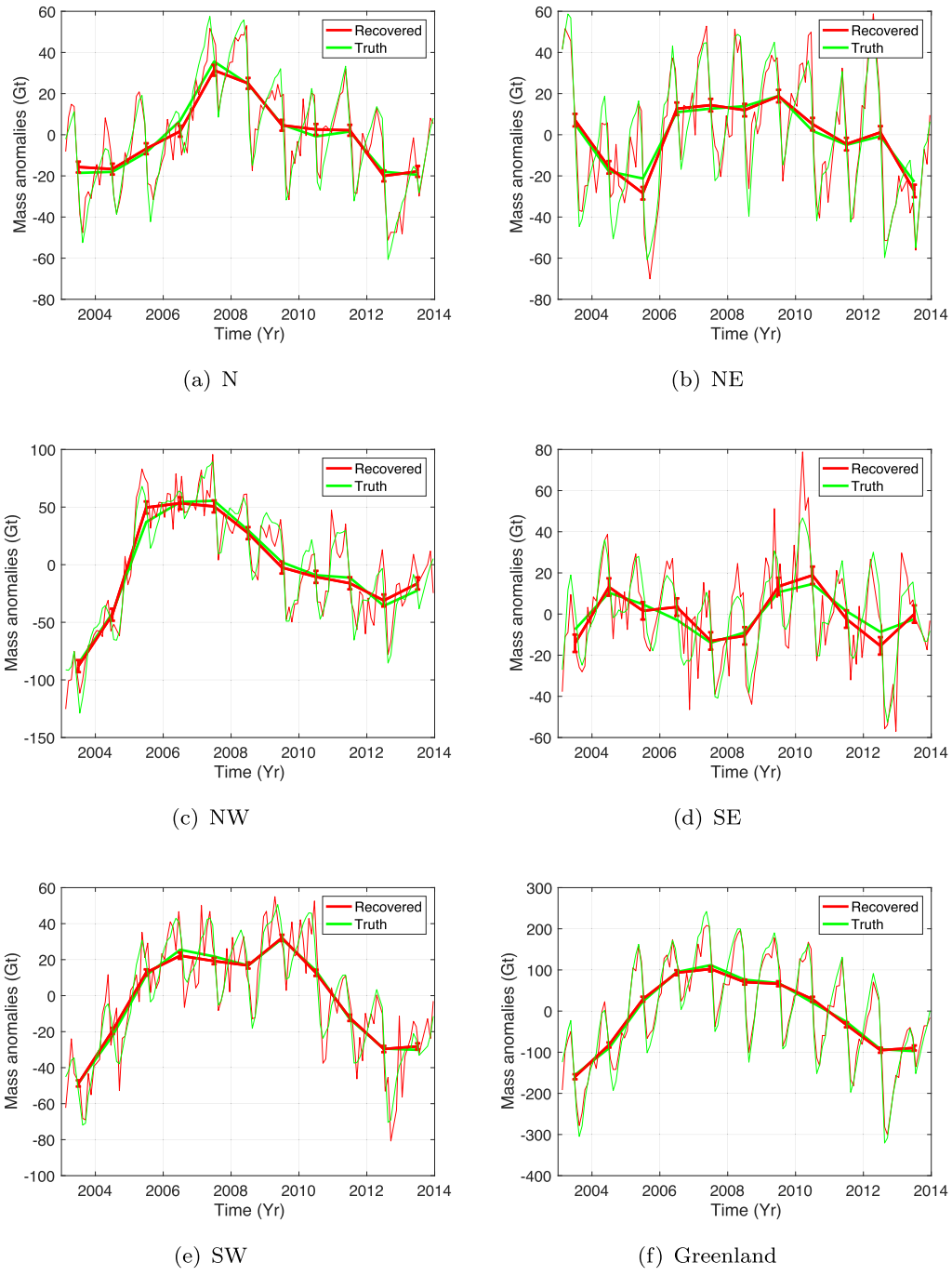


**Figure 10.** The regularized estimates of inter-annual mass variations and the 'true' ones obtained in the numerical study for each drainage system and for whole Greenland in the 23 mascon case. Data weighting is applied. The estimated and 'true' de-trended time-series are shown as a reference as dash lines. The rms difference between the 'true' and estimated values is shown as the error bar.

**Table 1.** The statistics of inter-annual mass variations estimated from synthetic data. The units are gigatransfers.

| | Data weighting | Number of mascons 6 | 8 | 12 | 23 | 36 | 54 |
|---|---|---|---|---|---|---|---|
| rms errors | Yes | 6.9 | 4.3 | 5.7 | 3.6 | 3.9 | 4.5 |
| rms errors | No | 7.1 | 6.0 | 6.3 | 4.7 | 5.2 | 5.2 |
| rms of the true mass anomalies | – | 25.7 | 21.5 | 23.1 | 21.4 | 21.5 | 22.3 |
| SNR | Yes | 3.7 | 5.0 | 4.0 | 6.0 | 5.6 | 5.0 |
| SNR | No | 3.6 | 3.6 | 3.7 | 4.6 | 4.1 | 4.3 |

Table 4. The uncertainties are taken over from the numerical study. Next, we compare our trend estimates with similar estimates from the CSR mascon product (Save *et al.* 2016), which used the same geometry of drainage systems. Note that the CSR mascon product is produced with incorporating spatial constraints in the form of a first-order Tikhonov regularization, whereas we apply a much simpler zero-order Tikhonov regularization. From Table 4, it can be found that our trend estimates for all drainage systems agree reasonably well with the estimates from CSR. The largest discrepancies (up to 15 Gt yr$^{-1}$) are observed for the N drainage system. We explain this

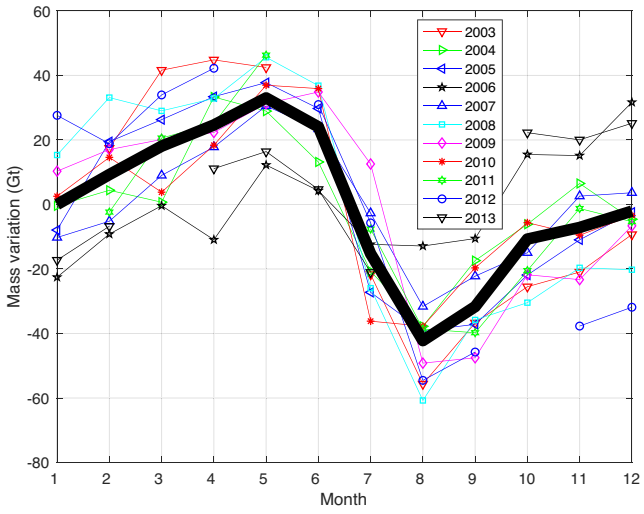


**Figure 11.** Mean true mass anomalies per calendar month in the numerical study, for the Northern (N) drainage system, $\overline{\overline{m}}^i$ (thick black curve). The thin curves represent monthly mass anomalies of individual years. The territory of Greenland was partitioned into 8 mascons.

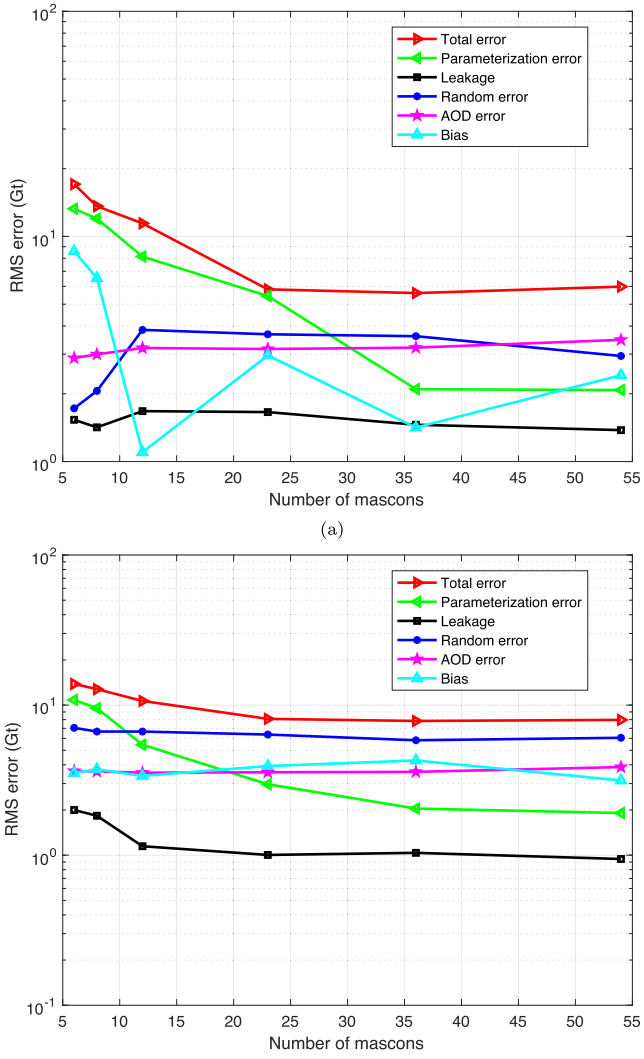


**Figure 12.** The rms errors in mean mass anomalies per calendar month (in units of gigatransfer) estimated with (a) and without (b) data weighting at drainage system scale, as functions of the number of mascons.

**Table 2.** The statistics of mean mass anomalies per calendar month estimated from synthetic data. The units are gigatransfer.

| | Data weighting | Number of mascons 6 | 8 | 12 | 23 | 36 | 54 |
|---|---|---|---|---|---|---|---|
| rms errors | Yes | 17.1 | 13.6 | 11.4 | 5.8 | 5.6 | 6.0 |
| rms errors | No | 13.8 | 12.8 | 10.7 | 8.1 | 7.8 | 8.0 |
| rms of the true mass anomalies | – | 31.0 | 31.9 | 31.0 | 33.1 | 33.1 | 34.6 |
| SNR | Yes | 1.8 | 2.3 | 2.7 | 5.7 | 5.9 | 5.8 |
| SNR | No | 2.2 | 2.5 | 2.9 | 4.1 | 4.2 | 4.3 |

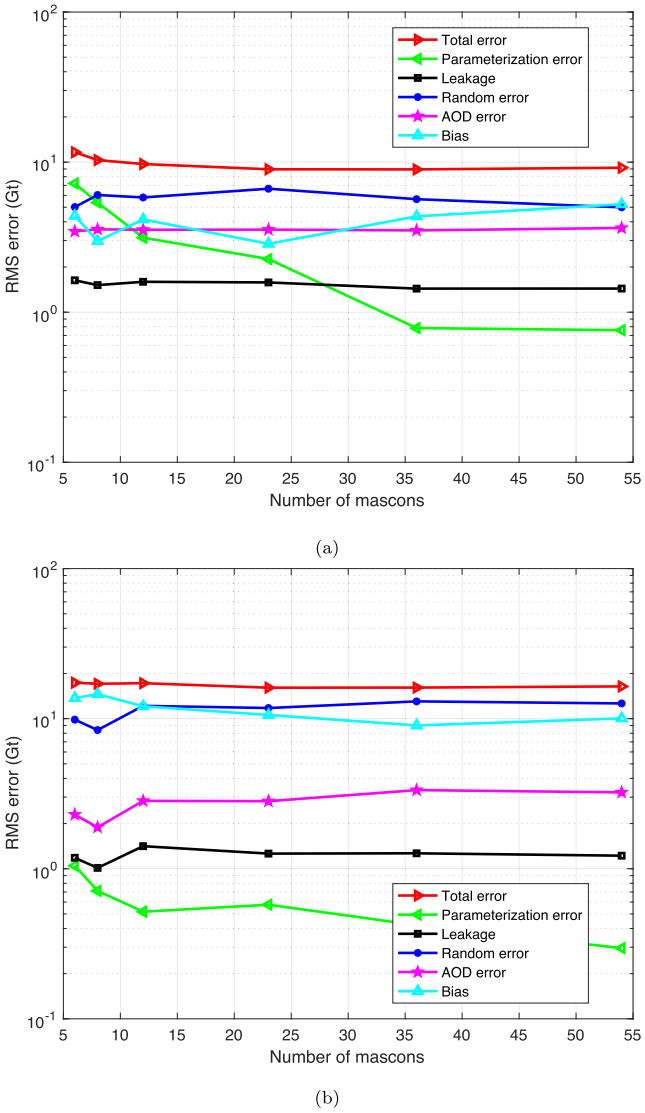


**Figure 13.** Total rms error and rms error per error source of monthly mass anomalies at drainage system scale in units of gigatransfers. Weighted least-squares estimator (a) versus ordinary least-squares estimator (b) as functions of the number of mascons.

**Table 3.** The statistics of monthly mass anomalies estimated from synthetic data. The units are gigatransfers.

| | Data weighting | Number of mascons 6 | 8 | 12 | 23 | 36 | 54 |
|---|---|---|---|---|---|---|---|
| rms errors | Yes | 11.6 | 10.3 | 9.7 | 9.0 | 8.9 | 9.2 |
| rms errors | No | 17.4 | 17.1 | 17.2 | 16.1 | 16.1 | 16.4 |
| rms of the true mass anomalies | – | 23.1 | 24.0 | 25.7 | 24.6 | 25.1 | 25.8 |
| SNR | Yes | 2.0 | 2.3 | 2.6 | 2.8 | 2.8 | 2.8 |
| SNR | No | 1.3 | 1.4 | 1.5 | 1.5 | 1.6 | 1.6 |

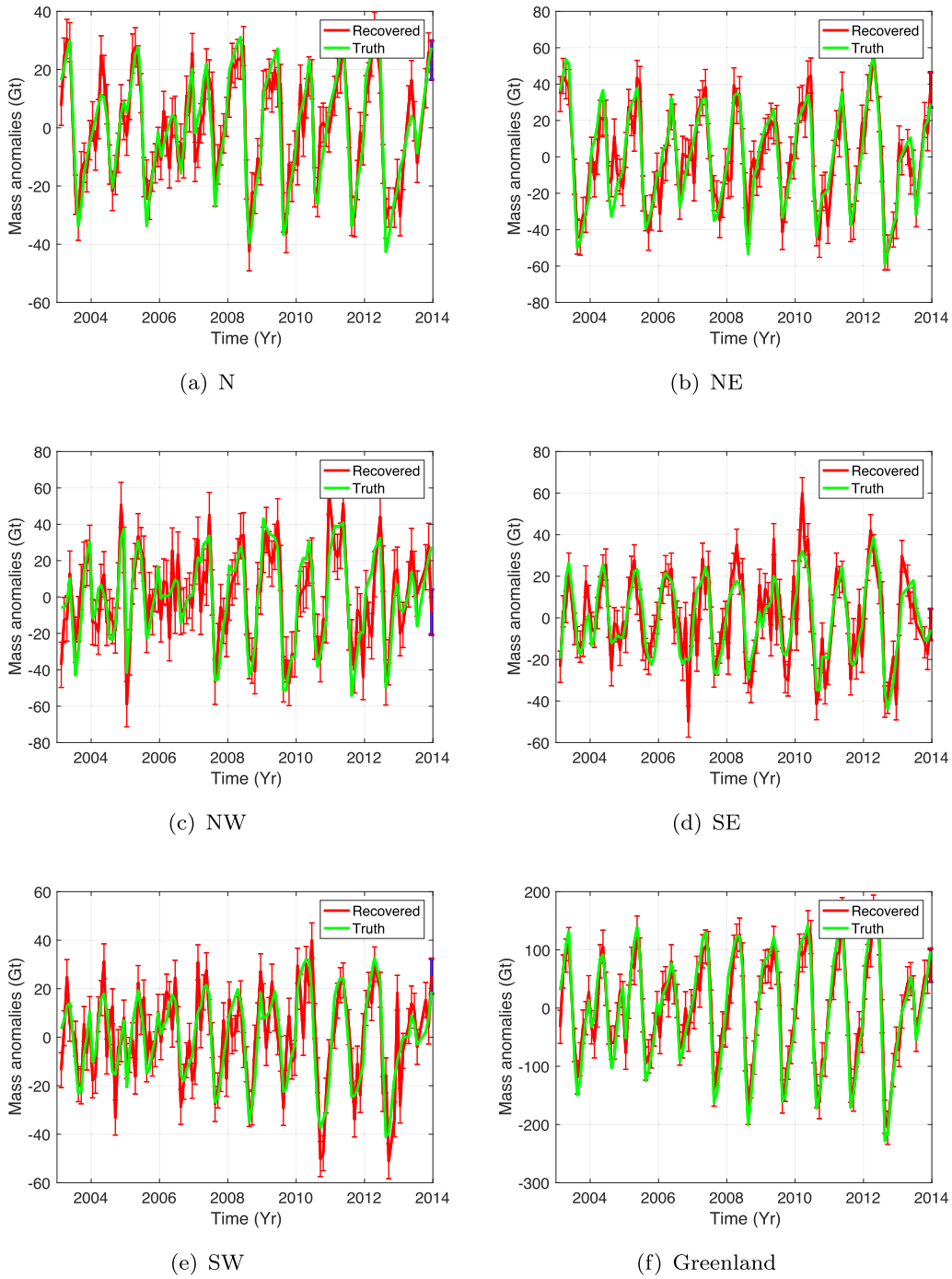


**Figure 14.** The regularized monthly mass anomaly time-series shown with $1-\sigma$ error bar and the 'true' ones in the numerical study for each drainage system and for whole Greenland in the 23 mascon case. Data weighting is applied. Note that the trend and inter-annual variabilities are removed.

**Table 4.** The trend estimates based on real GRACE data in the case of 23 mascons at the drainage system scale. The uncertainties of estimates with and without data weighting are based on the numerical study. For comparison, the trends from CSR mascon product are also shown. The units are Gt yr$^{-1}$.

| Method | N | NW | NE | SW | SE |
|---|---|---|---|---|---|
| With data weighting | $-9 \pm 11$ | $-94 \pm 1$ | $-18 \pm 3$ | $-32 \pm 5$ | $-83 \pm 6$ |
| Without data weighting | $-10 \pm 11$ | $-99 \pm 4$ | $-24 \pm 6$ | $-35 \pm 3$ | $-95 \pm 1$ |
| CSR | $-24$ | $-92$ | $-24$ | $-32$ | $-90$ |

by the usage of 120 km wide buffer zone in the preparation of the CSR mascon product (Save *et al.* 2016). This likely causes a signal leakage from nearby glaciers in Canada.

Then, we analyse the long-term trend estimates integrated over entire Greenland. We do not apply regularization in this case to minimize the biases in the obtained estimates. The results are shown in Fig. 15. The estimates obtained both with and without data weighting converge to a value of about $-281$ Gt yr$^{-1}$ when the number of mascons increases. Interestingly, the sensitivity of the estimated trend to the chosen parameterization is much stronger when no data

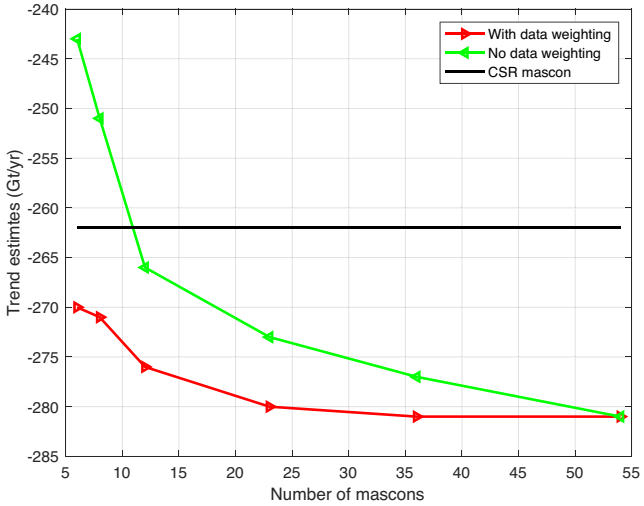


**Figure 15.** Mass anomaly trends over the period 2003–2013 in units of Gt yr$^{-1}$ estimated with and without data weighting from real GRACE data and integrated over entire Greenland, as functions of the number of mascons.

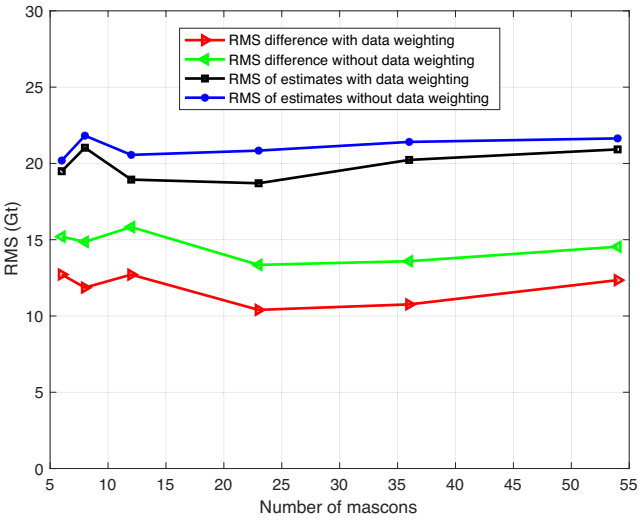


**Figure 16.** RMS differences (in units of Gt) between inter-annual mass variations from real GRACE data and from the RACMO2.3 output, as functions of the number of mascons. The rms inter-annual mass variations themselves are also shown as a reference.

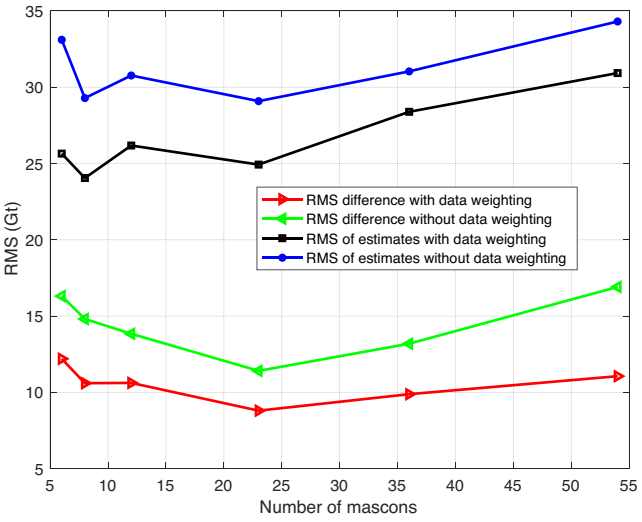


**Figure 17.** The rms difference (in units of gigatransfer) between mean mass anomaly estimates per calendar month from real GRACE data and from the RACMO2.3 output, as functions of the number of mascons. The rms mass anomalies themselves are also presented as a reference.

weighting is used; the estimate changes from $-243$ Gt yr$^{-1}$ for 6 mascons to $-281$ Gt yr$^{-1}$ for 54 mascons (15 per cent difference). When data weighting is applied, the difference between the 6- and 54-mascon solutions is only 12 Gt yr$^{-1}$ or 4 per cent. This finding is consistent with the numerical study in Section 3.2 (cf. Fig. 8), demonstrating that data weighting indeed makes the trend estimates less sensitive to the dominant parameterization errors when entire Greenland is considered.

In line with the synthetic study, we consider the trend estimate obtained with the largest number of mascons in the presence of data weighting as the most realistic and accurate one. This estimate, that is, $-281 \pm 2$ Gt yr$^{-1}$, is close to the estimates over the same period (i.e., 2003–2013) published in literature: $-280 \pm 58$ Gt yr$^{-1}$ in Velicogna *et al.* (2014) and $-278 \pm 19$ Gt yr$^{-1}$ in Schrama *et al.* (2014). In addition, it is likely that the trend estimated by CSR mascon contains a bias (see Fig. 15). Note that the uncertainty of our trend estimate for the whole ice sheet is obtained as the root-sum-square of the individual error sources in the numerical study. However, there are also other errors that were not considered in the numerical study but may play a role in the context of real data processing (Ran *et al.* 2018b). This includes uncertainties related to the parameterization of the ocean areas around Greenland (i.e., the leakage of minor ocean signals around Greenland) and GIA. By taking all those uncertainties into account, we estimate the total error of the trend estimate as 11 Gt yr$^{-1}$.

### 4.2 Analysis of the estimates at the intermediate and short timescales

In addition, we investigate the impact of the parameterization on the other quantities of interests, that is, inter-annual mass variations, mean mass anomalies per calendar month and monthly mass anomalies. For this purpose, we compare the estimates from real GRACE data with the output of RACMO2.3 model (Noël *et al.* 2015). In doing so, we assume that ice discharge manifests itself in GRACE data as only a long-term trend, so that the remaining mass anomalies observed by GRACE are dominated by SMB (van den Broeke *et al.* 2009). Therefore, we de-trend the mass anomaly time-series from both GRACE and RACMO2.3 to make them comparable.

First, we examine the inter-annual mass variations. The corresponding RMS differences between GRACE and RACMO-based estimates are shown in Fig. 16 as functions of the number of mascons. In order to understand the noise level better, the rms of estimates are also shown for a comparison. The rms differences decreases from 6 to 23 mascons, followed by a slightly increase over 23–54 mascons. The best agreement with RACMO is obtained in the 23 mascon case when the data weighting is applied. All these findings are consistent with those based on the numerical study, indicating a realistic setup of the latter.

Next, the mean mass anomalies per calendar month are investigated. The rms differences between the GRACE- and RACMO-based estimates are shown in Fig. 17. The rms differences for 23–

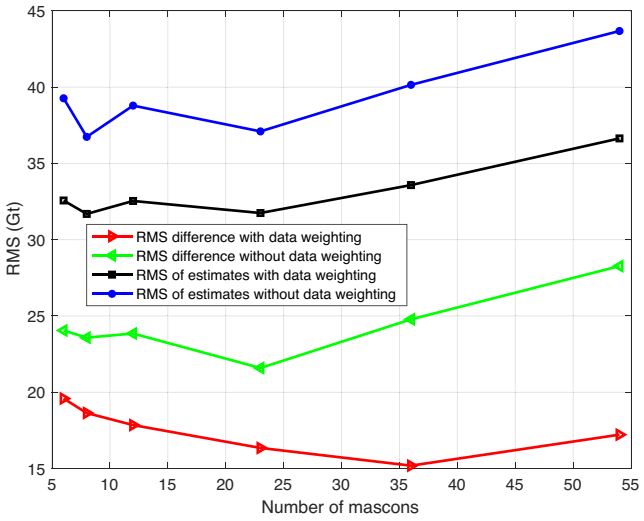


**Figure 18.** The rms difference (in units of Gt) between monthly mass anomalies from real GRACE data and from the RACMO2.3 output, as functions of the number of mascons. The rms monthly mass anomalies themselves are also shown as a reference.

54 mascons are comparable, while they slightly increase when the number of mascon decreases from 23 to 6, no matter whether data weighting is applied or not. The data weighting scheme notably reduces the rms differences (by ∼18 per cent). All this is also in agreement with the numerical study.

Furthermore, the monthly mass anomaly estimates are analysed. Fig. 18 shows the rms differences between the GRACE- and RACMO-based time-series at the drainage system scale. In absolute terms, the rms differences in the absence of data weighting are about 15 per cent larger than those obtained after data weighting was applied. When using data weighting, the smallest rms difference is observed with 36 mascons, whereas the smallest one is found with the 23 mascons without data weighting. However, the discrepancies of rms differences over various parameterizations are minor, no matter whether data weighting is applied or not.

Finally, after removing the trends and accelerations, we perform a comparison of our estimated time-series with the CSR mascon product (Save *et al.* 2016), and validate with independent data: SMB output from RACMO2.3. As discussed earlier, in general, the mass anomalies estimated with 23 mascons and data weighting are of the highest quality. Therefore, just those mass anomalies are compared considered (see Fig. 19). The error bars in Fig. 19 are computed as root-sum-squared errors of two types: mean mass per calendar month and monthly mass anomalies, based on the numerical study. Note that errors in the trend estimates is not included, because the time-series are de-trended. Next we perform the statistical analysis of the differences between the CSR mascon product and the RACMO-base estimates. The rms differences of inter-annual mass variations, mean mass anomalies per calendar month, and monthly mass anomalies are at a level comparable to that of our estimates, provided that the data weighting is applied (see Table 5).

## 5 CONCLUSIONS

In this study, we analysed the impact of the chosen parameterization on the mass anomaly estimates from GRACE data when the mascon approach with or without data weighting is applied. The zero-order Tikhonov regularization was applied in the data inversion. We analysed the impact at different temporal scales by considering long-term linear trends, interannual mass variations, mean mass anomalies per calendar month and time-series of monthly mass anomalies. Both synthetic and real GRACE data were considered.

In the simulation study, errors of four types (i.e., parameterization error, random error, leakage and AOD error) were simulated. In this way, we found that the parameterization error and the random error, as well as the bias introduced by regularization, are the major contributors to the overall error budget of the estimates produced both with and without data weighting. For long-term linear trend estimates, the parameterization error is the dominant error type. This is due to a significant reduction of the random noise when estimating a linear trend by using a large number of monthly solutions as input. For inter-annual mass variations and mean mass per calendar month, the parameterization error is dominant when the number of mascons is small; when increasing the number of mascons, the random error takes over. For monthly mass anomalies, the random error is the most critical error type for almost all parameterizations. This is consistent with the fact that the usage of data weighting (which is designed to suppress random noise) is effective in all the scenarios, except for the estimation of long-trend at the drainage system scale. The AOD error and the leakage error are minor contributors to the overall error budget no matter what temporal scales are considered.

Remarkably, we found that the best estimates of the long-term linear trends integrated over entire Greenland are obtained when the number of mascons is large, whereas the regularization is not applied. This can be explained by the fact that random noise is subject to strong spatial correlations and is efficiently averaged out when the estimates are integrated over entire Greenland. On the other hand, the usage of a large number of mascons suppresses the other important contributor to the error budget, that is, parameterization error. In that situation, the regularization is not advised, since the bias introduced by the regularization is not compensated by a reduction of errors.

We applied our findings to process real GRACE data. First, the long-term linear trend over the period 2003–2013 for entire Greenland was estimated to be around $-281$ Gt yr$^{-1}$. This value agrees well with earlier trend estimates in Schrama *et al.* (2014) and Velicogna *et al.* (2014). In the numerical study, we found that the estimates for entire Greenland suffer from only minor errors (i.e., 0.8 Gt yr$^{-1}$ with data weighting and 2 Gt yr$^{-1}$ without data weighting). Note that the uncertainty of the trend estimates might be larger in reality, since there are other error sources, for example, GIA, sea level rise, etc.

We also considered the mass anomaly estimates at intermediate and short timescales using rms differences between de-trended timeseries from GRACE and from the RACMO2.3 model. These differences, as well as the results based on synthetic data, drew us to the conclusions that (i) the optimal data weighting based on full error covariance matrices of GRACE solutions is advised and (ii) the optimal way to parameterize the territory of Greenland is to split it into 23 mascons (the area of each one being ∼90 000 km$^2$). Smaller mascons may slightly worsen the estimated of inter-annual variations, whereas larger mascons yield inferior results in most of the cases considered (the latter can be explained by the impact of the parameterization errors). Similar recommendations apply also to the trends estimates at the drainage system scale, with an exception that the aforementioned optimal data weighting is not needed.

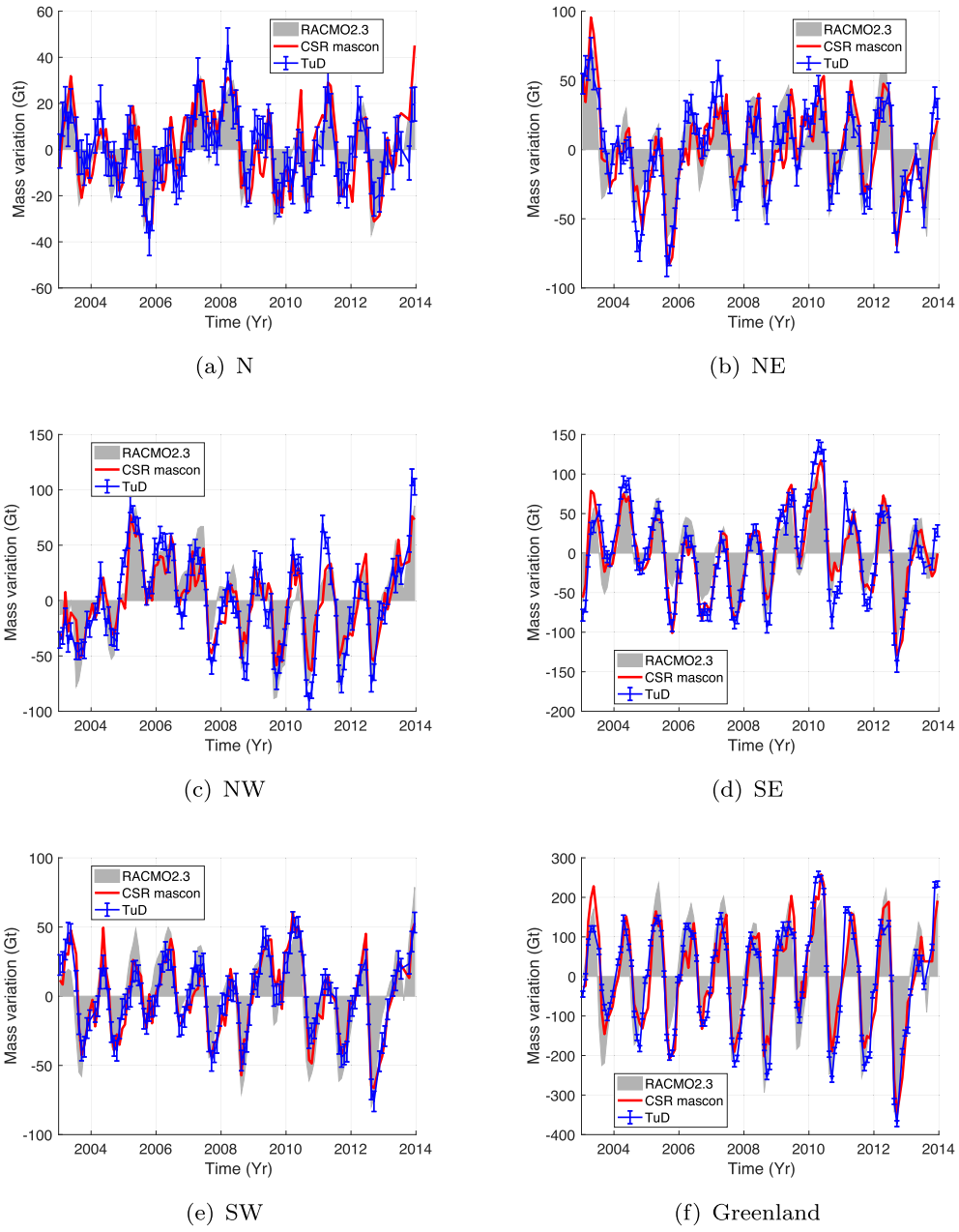


**Figure 19.** Mass anomaly time-series for each drainage system and for whole Greenland estimated with data weighting, in the case of 23 mascons. Note that the long-term linear trends are removed. The uncertainties $(1-\sigma)$ are computed based on the numerical study.

**Table 5.** The rms differences between a GRACE solution and the RACMO2.3 output in terms of inter-annual mass variations mean mass anomalies per calendar month and monthly mass anomalies. The units are gigatransfers.

| GRACE solution | rms difference of inter-annual mass anomalies | rms differences of mean mass per calendar month | rms differences of monthly mass anomalies |
|---|---|---|---|
| This study (with data weighting) | 9 | 10 | 16 |
| This study (without data weighting) | 11 | 13 | 22 |
| CSR | 9 | 11 | 15 |

## ACKNOWLEDGEMENTS

We thank the editor and two reviewers: Dr. Jennifer Bonin and Dr. Shuang Yi for their constructive comments, which dramatically improve the quality of this manuscript. We would like to thank the CSRat University of Texas, Austin for providing GRACE Level-2 data and the corresponding error variance–covariance matrices. We also thank Dr. B. Gunter, who provided us with the GrIS elevation change rates over 2003–2009 estimated from ICESat data. Noël B. and van den Broeke M.R. are acknowledged for providing SMB estimates produced with RACMO 2.3. We would also acknowledge the usage of available C20 and degree-1 coefficients that were produced by Swenson *et al.* (2008) and Cheng *et al.* (2013), respectively. JR thanks his sponsor, the Chinese Scholarship Council. JR has also been partly supported by the National Natural Science Foundation

of China (41774094, 41431070 and 41674084) and the Strategic Priority Research Program of the Chinese Academy of Sciences (XDB23030100).

## REFERENCES


A, G., Wahr, J. & Zhong, S., 2013. Computations of the viscoelastic response of a 3-D compressible Earth to surface loading: an application to glacial isostatic adjustment in Antarctica and Canada, *Geophys. J. Int.,* **192**(2), 557–572.

Baur, O. & Sneeuw, N., 2011. Assessing Greenland ice mass loss by means of point-mass modeling: a viable methodology, *J. Geod.,* **85**(9), 607–615.

Bonin, J. & Chambers, D., 2013. Uncertainty estimates of a GRACE inversion modelling technique over Greenland using a simulation, *Geophys. J. Int.,* **194**(1), 212–229.

Chen, J.L., Wilson, C.R. & Tapley, B.D., 2006. Satellite gravity measurements confirm accelerated melting of Greenland ice sheet, *Science,* **313**(5795), 1958–1960.

Cheng, M., Tapley, B.D. & Ries, J.C., 2013. Deceleration in the Earth's oblateness, *J. geophys. Res.,* **118**(2), 740–747.

Ditmar, P., Teixeira da Encarnação, J.H. & Farahani, H., 2012. Understanding data noise in gravity field recovery on the basis of inter-satellite ranging measurements acquired by the satellite gravimetry mission GRACE, *J. Geod.,* **86**(6), 441–465.

Dobslaw, H., Flechtner, F., Bergmann-Wolf, I., Dahle, C., Dill, R., Esselborn, S., Sasgen, I. & Thomas, M., 2013. Simulating high-frequency atmosphere-ocean mass variability for dealiasing of satellite gravity observations: AOD1B RL05, *J. geophys. Res.,* **118**(7), 3704–3711.

Felikson, D., Urban, T.J., Gunter, B.C., Pie, N., Pritchard, H.D., Harpold, R. & Schutz, B.E., 2017. Comparison of elevation change detection methods from icesat altimetry over the greenland ice sheet, *IEEE Trans. Geosci. Remote Sens.,* **55**(10), 1–12.

eds Forsberg, R. & Reeh, N., 2007, Mass change of the Greenland Ice Sheet from GRACE, Harita Dergisi, Ankara, gravity field of the Earth, in: *Proceedings of the 1st Meeting of the Int. Gravity Field Service,* 73 pp.,

Hansen, P.C., 1992. Analysis of discrete ill-posed problems by means of the l-curve, *SIAM Rev.,* **34**(4), 561–580.

Jacob, T., Wahr, J., Pfeffer, W. & Swenson, S., 2012. Recent contributions of glaciers and ice caps to sea level rise, *Nature,* **482**(7386), 514–518.

Khan, S.A., Aschwanden, A., Bjørk, A.A., Wahr, J., Kjeldsen, K.K. & Kjaer, K.H., 2015. Greenland ice sheet mass balance: a review, *Rep. Prog. Phys.,* **046801,** 1–26.

Luthcke, S.B. *et al.*, 2006. Recent Greenland ice mass loss by drainage system from satellite gravity observations, *Science,* **314,** 1286–1289.

Luthcke, S.B., Sabaka, T.J., Loomis, B.D., Arendt, A.A., McCarthy, J.J. & Camp, J., 2013. Antarctica, Greenland and Gulf of Alaska land-ice evolution from an iterated GRACE global mascon solution, *J. Glaciol.,* **59**(216), 613–631.

Noël, B., van de Berg, W.J., van Meijgaard, E., Kuipers Munneke, P., van de Wal, R.S.W. & van den Broeke, M.R., 2015. Evaluation of the updated regional climate model RACMO2.3: summer snowfall impact on the Greenland Ice Sheet, *Cryosphere,* **9**(5), 1831–1844.

Ran, J., 2017. Analysis of mass variations in Greenland by a novel variant of the mascon approach, *PhD thesis,* Delft University of Technology.

Ran, J., Ditmar, P., Klees, R. & Farahani, H.H., 2018a. Statistically optimal estimation of Greenland Ice Sheet mass variations from GRACE monthly solutions using an improved mascon approach, *J. Geod.,* **92**(3), 299–319.

Ran, J. *et al.*, 2018b. Seasonal mass variations show timing and magnitude of meltwater storage in the greenland ice sheet, *Cryosphere Discuss.,* **2018,** 1–30.

Rowlands, D.D., Luthcke, S.B., Klosko, S.M., Lemoine, F.G.R., Chinn, D.S., McCarthy, J.J., Cox, C.M. & Anderson, O.B., 2005. Resolving mass flux at high spatial and temporal resolution using GRACE intersatellite measurements, *Geophys. Res. Lett.,* **32**(4), 1–4.

Save, H., Bettadpur, S. & Tapley, B.D., 2016. High-resolution CSR GRACE RL05 mascons, *J. geophys. Res.,* **121**(10), 7547–7569.

Schrama, E.J.O. & Wouters, B., 2011. Revisiting Greenland Ice Sheet mass loss observed by GRACE, *J. geophys. Res.,* **116**(2), B02407, doi:10.1029/2009JB006847.

Schrama, E.J.O., Wouters, B. & Rietbroek, R., 2014. A mascon approach to assess ice sheet and glacier mass balances and their uncertainties from GRACE data, *J. geophys. Res.,* **119**(7), 6048–6066.

Shepherd, A. *et al.*, 2012. A reconciled estimate of ice-sheet mass balance, *Science,* **338**(6111), 1183–1189.

Stedinger, J.R. & Tasker, G.D., 1986. Regional hydrologic analysis, 2, model-error estimators, estimation of sigma and log-pearson type 3 distributions, *Water Resour. Res.,* **22**(10), 1487–1499.

Stocker, T.F. *et al.*, 2013, Climate change 2013: the physical science basis, Tech. rep., 1535 pp.

Swenson, S., 2012, Grace monthly land water mass grids netcdf release 5.0. ver. 5.0., PO. DAAC, CA, USA Dataset accessed [2016-12-01] at http://dx.doi.org/10.5067/TELND-NC005, 10.

Swenson, S., Chambers, D. & Wahr, J., 2008. Estimating geocenter variations from a combination of GRACE and ocean model output, *J. geophys. Res.,* **113**(B8), B08410, doi:10.1029/2007JB005338.

Thompson, P.F., Bettadpur, S. & Tapley, B.D., 2004. Impact of short period, non-tidal, temporal mass variability on GRACE gravity estimates, *Geophys. Res. Lett.,* **31**(6), L06619, doi:10.1029/2003GL019285.

van den Broeke, M. *et al.*, 2009. Partitioning recent Greenland mass loss, *Science,* **326**(5955), 984–986.

Velicogna, I., 2009. Increasing rates of ice mass loss from the Greenland and Antarctic ice sheets revealed by GRACE, *Geophys. Res. Lett.,* **36**(19), L19503.

Velicogna, I. & Wahr, J., 2006. Acceleration of Greenland ice mass loss in spring 2004, *Nature,* **443**(7109), 329–331.

Velicogna, I., Sutterley, T.C. & vanden Broeke, M.R., 2014. Regional acceleration in ice mass loss from greenland and antarctica using grace time-variable gravity data, *Geophys. Res. Lett.,* **41**(22), 8130–8137.

Wahr, J., Wingham, D. & Bentley, C., 2000. A method of combining ICESat and GRACE satellite data to constrain Antarctic mass balance, *J. geophys. Res.,* **105**(B7), 16 279–16 294.

Watkins, M.M., Wiese, D.N., Yuan, D.-N., Boening, C. & Landerer, F.W., 2015. Improved methods for observing Earth's time variable mass distribution with GRACE using spherical cap mascons, *J. geophys. Res.,* **120**(4), 2648–2671.

Xu, G., 2010. *Sciences of Geodesy-I: Advances and Future Directions,* Springer Science & Business Media.

Yi, S., Wang, Q. & Sun, W., 2016. Basin mass dynamic changes in China from GRACE based on a multibasin inversion method, *J. geophys. Res.,* **121**(5), 3782–3803.

Zwally, H.J., Giovinetto, M.B., Beckley, M.A. & Saba, J.L., 2012. 'Antarctic and Greenland drainage systems'. GSFC Cryospheric Sciences Laboratory. Available at: icesat4.gsfc.nasa.gov/cryo_data/ant_grn_drainage_systems.php, Last accessed: Dec 2015.